

Rainfall Estimation with a Polarimetric Prototype of WSR-88D

ALEXANDER V. RYZHKOV, SCOTT E. GIANGRANDE, AND TERRY J. SCHUUR

Cooperative Institute for Mesoscale Meteorological Studies, University of Oklahoma, Norman, Oklahoma

(Manuscript received 26 April 2004, in final form 3 October 2004)

ABSTRACT

As part of the Joint Polarization Experiment (JPOLE), the National Severe Storms Laboratory conducted an operational demonstration of the polarimetric utility of the Norman, Oklahoma (KOUN), Weather Surveillance Radar-1988 Doppler (WSR-88D). The capability of the KOUN radar to estimate rainfall is tested on a large dataset representing different seasons and different types of rain. A dense gauge network—the Agricultural Research Service (ARS) Micronet—is used to validate different polarimetric algorithms for rainfall estimation. One-hour rain totals are estimated from the KOUN radar using conventional and polarimetric algorithms and are compared with hourly accumulations measured by the gauges. Both point and areal rain estimates are examined. A new “synthetic” rainfall algorithm has been developed for rainfall estimation. The use of the synthetic polarimetric algorithm results in significant reduction in the rms errors of hourly rain estimates when compared with the conventional nonpolarimetric relation: 1.7 times for point measurements and 3.7 times for areal rainfall measurements.

1. Introduction

Improvement of quantitative precipitation estimation (QPE) is one of the primary benefits of a dual-polarization radar. In addition to conventional radar reflectivity factor Z , a polarimetric radar is capable of measuring the differential reflectivity Z_{DR} , specific differential phase K_{DP} , and the cross-correlation coefficient ρ_{hv} between two orthogonally polarized radar returns. Using multiparameter radar information instead of radar reflectivity alone helps to significantly improve the radar data quality, distinguish rain echoes from the radar signals caused by other scatterers (snow, ground clutter, insects, birds, chaff, etc.), and to reduce the impact of drop size distribution (DSD) variability on the quality of rainfall estimation. Differential reflectivity Z_{DR} is a good measure of the median drop diameter that should be taken into account for more accurate rain measurements. Among the indisputable advantages of polarimetric rainfall estimation, based on specific differential phase K_{DP} , is its immunity to radar miscalibration, attenuation in precipitation, and partial blockage of radar beam (Zrnic and Ryzhkov 1996).

Several different polarimetric relations for rain rate estimation have been suggested during the last two decades. These relations utilize Z , Z_{DR} , and K_{DP} in dif-

ferent combinations. The relations were obtained for different radar wavelengths using either simulated or measured DSDs and various assumptions about the shape dependence of raindrops on their size. The performance of many suggested polarimetric rainfall estimation techniques has been tested on several extended datasets from Oklahoma (Ryzhkov and Zrnic 1996; Ryzhkov et al. 2000; Ryzhkov et al. 2001), Colorado, Kansas (Brandes et al. 2001), and Florida (Brandes et al. 2002, hereinafter BZV02) for S-band radars; Australia (May et al. 1999) for C-band radar; and Virginia (Matrosov et al. 2002) for X-band radar.

All of the above validation studies have shown that (a) there is an improvement in rainfall estimation if a dual-polarization radar is used, and (b) polarimetric rainfall estimation techniques are more robust with respect to DSD variations than are the conventional $R(Z)$ relations. At the moment, however, there is no consensus on the degree of improvement and the choice of an optimal polarization relation.

As part of the continuous modernization of the nationwide Weather Surveillance Radar-1988 Doppler (WSR-88D) network, the U.S. National Weather Service (NWS) has decided to add polarimetric capability to existing operational radars. The proof of concept was tested on the National Severe Storms Laboratory (NSSL) research WSR-88D in Norman, Oklahoma (KOUN radar hereinafter), which was polarimetrically upgraded in March 2002. The polarimetric Next Generation Weather Radar (NEXRAD) prototype was designed to simultaneously transmit and receive horizon-

Corresponding author address: Alexander V. Ryzhkov, CIMMS/NSSL, 1313 Halley Circle, Norman, OK 73069.
E-mail: alexander.ryzhkov@noaa.gov

tally (H) and vertically (V) polarized waves (Doviak et al. 2000).

During 2002–03, the NSSL conducted an operational demonstration of the polarimetric utility of the KOUN WSR-88D. This demonstration project, referred as the Joint Polarization Experiment (JPOLE), sought to evaluate the engineering design of the polarimetric WSR-88D and demonstrate the utility of the radar data and products, including rainfall estimation and hydro-meteor classification.

A major objective of this study is to test existing conventional and polarimetric relations for rainfall estimation on a large dataset that was obtained during JPOLE and to develop an algorithm that is optimal and robust for the operational environment. Rainfall products from the polarimetric KOUN WSR-88D are validated using the Agricultural Research Service (ARS) Micronet, consisting of 42 rain gauges, with an average spacing of 5 km (Fig. 1). This network is well calibrated and provides 5-min rain accumulation data. The data collected by the conventional KTLX WSR-88D (located about 20 km from the polarimetric prototype) were used to validate calibration of radar reflectivity measured by the KOUN radar.

The ARS gauges are located at the ranges of 50–88 and 70–108 km from the KOUN and Oklahoma City, Oklahoma (KTLX), radars, respectively. At such distances, the performance of radar-rainfall algorithms over the ARS test area is mostly affected by DSD variability and the possible presence of hail rather than ground clutter and brightband contamination (even during cold season in Oklahoma). Therefore, the ARS Micronet primarily serves as a validation tool to optimize polarimetric rainfall estimation at relatively close distances from the radar where the first two factors are most important. Evaluation of polarimetric rain measurements at longer distances from the radar is a subject of separate studies (Giangrande and Ryzhkov 2003; Ryzhkov et al. 2003).

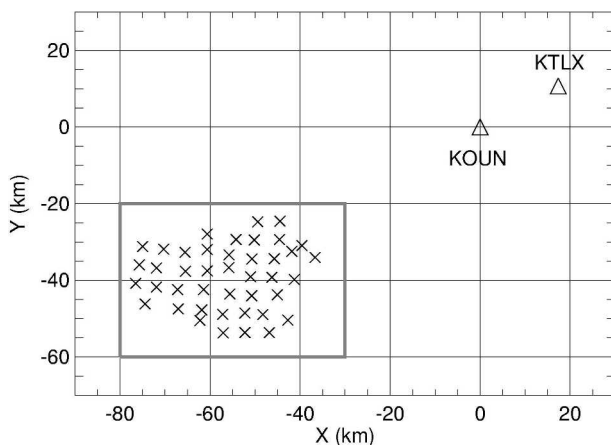


FIG. 1. Radar locations with respect to the ARS Micronet gauges (crosses).

2. Radar dataset

We collected polarimetric KOUN radar data from April 2002 through July 2003. In total, 98 events were cataloged both chronologically and by event type, and subsequently were described within an online database (available at <http://cimms.ou.edu/~heinsel/jpole/database.html> and <http://cimms.ou.edu/~heinsel/jpole/stormtype.html>, respectively).

A data subset, consisting of 24 rain events with 50 h of observations for which the ARS gauges recorded a sizeable amount of precipitation, was selected for in-depth analysis. This subset contains 18 convective and 6 stratiform rain events observed from June 2002 to June 2003. Both “warm season” and “cold season” rain events are well represented in the dataset. Cold-season stratiform rain with a relatively low bright band mostly occurred in the month of October 2002.

Radar reflectivity Z , differential reflectivity Z_{DR} , differential phase Φ_{DP} , and the cross-correlation coefficient ρ_{hv} were estimated with a radial resolution of 0.267 km using a short dwell time (48 radar samples) in order to satisfy the NEXRAD requirement for rapid antenna rotation rate (3 rpm) and azimuthal resolution (1°).

Absolute calibration of Z for the KOUN radar was performed either by matching the 1-h areal rainfall estimate using the standard NEXRAD $R(Z)$ algorithm with the one obtained from the operational KTLX radar, or by applying a polarimetric consistency technique (Gorgucci et al. 1999) recently modified by Ryzhkov et al. (2005) if simultaneous KTLX data were not available. The latter capitalizes on the interdependence of Z , Z_{DR} , and K_{DP} in the rain medium. Radar reflectivity biases retrieved with these two methods usually did not differ by more than 1 dB (Ryzhkov et al. 2005).

Absolute calibration of Z_{DR} was conducted using measurements of solar radiation in the orthogonal H and V channels and polarimetric properties of dry aggregated snow that was observed at high elevation angles (Melnikov et al. 2003; Ryzhkov et al. 2005).

Polarimetric radar data are processed in the following order:

- 1) Using averaging windows of three gates for Z and five gates for Z_{DR} and ρ_{hv} , Z , Z_{DR} , and ρ_{hv} are smoothed along the radial.
- 2) Both Z_{DR} and ρ_{hv} are corrected for noises in the two orthogonal channels. This is because both variables are negatively biased if the signal-to-noise ratio is less than 20 dB (Bringi and Chandrasekar 2001, hereinafter BC01).
- 3) Total differential phase Φ_{DP} is edited, unfolded, and smoothed along the radial using two averaging windows, corresponding to 9 and 25 successive gates. Thus, “lightly filtered” and “heavily filtered” radial profiles of Φ_{DP} are obtained.
- 4) Both Z and Z_{DR} are corrected for attenuation using heavily filtered Φ_{DP} and simple relations ΔZ (dB) =

$0.04\Phi_{\text{DP}}$ (degrees) and ΔZ_{DR} (dB) = $0.004\Phi_{\text{DP}}$ (degrees) (Ryzhkov and Zrnic 1995).

- 5) Two estimates of specific differential phase K_{DP} are obtained from the filtered Φ_{DP} as a slope of a least squares fit for two range averaging intervals, corresponding to 9 and 25 successive gates. For any particular range gate, the lightly filtered estimate of K_{DP} is selected if $Z > 40$ dBZ, and, otherwise, the heavily filtered estimate is used (Ryzhkov and Zrnic 1996). Thus, radial resolution of the K_{DP} estimate is about 6 km for relatively light rain ($R < 12$ mm h⁻¹) and about 2 km for more intense rain.

3. Radar-rainfall algorithms

As a basic conventional algorithm for radar-rainfall estimation we use the standard NEXRAD relation

$$R(Z) = 1.70 \times 10^{-2} Z^{0.714} \quad (1)$$

(i.e., inversion of the formula $Z = 300R^{1.4}$), where Z is expressed in mm⁶ m⁻³, and R is in mm h⁻¹. Values of Z are subject to a threshold at the level of 53 dBZ in order to mitigate hail contamination.

Two groups of polarimetric rainfall algorithms have been tested. One group includes the most recent power-law $R(K_{\text{DP}})$, $R(Z, Z_{\text{DR}})$, and $R(K_{\text{DP}}, Z_{\text{DR}})$ relations that we have found in the literature for S-band radars. Another group consists of similar algorithms that were derived using multiyear statistics of DSD measurements in central Oklahoma, with the following three different assumptions about raindrop shapes: 1) equilibrium shapes defined by Beard and Chuang (1987), 2) “oscillating raindrop” shapes from Bringi et al. (2003), and 3) shapes specified by BZV02.

The equilibrium raindrop shapes in steady airflow are defined by the following relation between the raindrop axis ratio a/b and its equivolume diameter D (mm):

$$a/b = 1.0048 + 0.00057D - 0.02628D^2 + 0.003682D^3 - 0.0001677D^4. \quad (2)$$

The actual shapes of raindrops in unsteady flow are expected to differ from the equilibrium shapes because of drop oscillations. Laboratory studies by Andsager et al. (1999) indicate that the shape of raindrops in the size range between 1.1 and 4.4 mm is better described by the formula

$$a/b = 1.012 - 0.01445D - 0.01028D^2. \quad (3)$$

Bringi et al. (2003) suggested using Eq. (3) for drops with sizes smaller than 4.4 mm and Eq. (2) for larger sizes. Another shape–diameter relation that combines the observations of different authors was recently proposed by BZV02,

$$a/b = 0.9951 + 0.02510D - 0.03644D^2 + 0.005303D^3 - 0.0002492D^4. \quad (4)$$

The dependencies of the raindrop axis ratio on its equivolume diameter for equilibrium shapes defined by (2), “oscillating” raindrop shapes specified by Bringi et al. (2003), and the ones defined by (4) are shown in Fig. 2.

In all simulations, it was assumed that the drops are canted with the mean canting angle equal to zero and the width of the canting angle distribution of 10°. The 25 920 one-minute DSDs that were measured with the NSSL’s 2D video disdrometer in 1998–2004 have been used for the computation of radar variables and the derivation of polarimetric relations for rainfall estimation (Schuur et al. 2001).

A list of tested polarimetric algorithms is presented in Table 1. The notation Z_{dr} is used for differential reflectivity expressed in linear scale, whereas Z_{DR} is expressed in logarithmic units (BC01; BZV02; and Illingworth and Blackman 2002, hereinafter IB02). The Goddard’s axis ratio used in the IB02 study is given by the formula (Goddard et al. 1995)

$$a/b = 1.075 - 0.065D - 0.0036D^2 + 0.0004D^3. \quad (5)$$

In the course of this study, 1-h rain totals that were obtained from the radars and gauges were compared. We examined both “point” and “areal” estimates of the one-hour rain accumulation. By point estimate we mean an hourly total averaged over a small (1 km × 1°) area centered on an individual gauge. Areal mean hourly total or areal mean rain rate is determined as a sum of hourly accumulations from all gauges that recorded rain divided by the number of such gauges.

After calibrating, editing, smoothing, and correcting for noise and attenuation of the raw radar data (as described in section 2), the following operations are

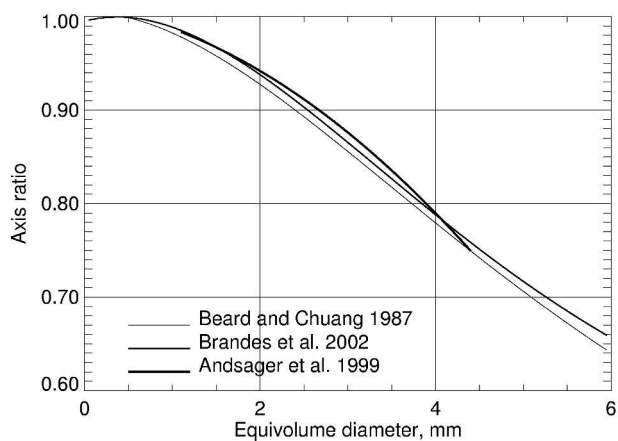


FIG. 2. Different dependencies of the raindrop axis ratio on the equivolume diameter.

TABLE 1. List of different polarimetric algorithms used for rainfall estimation.

$R(K_{DP}) = a K_{DP} ^b \text{sign}(K_{DP})$					
	a	b		Assumptions	Source
1	50.7	0.85		Simulated DSD, equilibrium shape	BC01
2	54.3	0.806		Measured DSD (FL), Brandes' shape	BZV02
3	51.6	0.71		Simulated DSD, Goddard's shape	IB02
4	44.0	0.822		Measured DSD (OK), equilibrium shape	NSSL
5	50.3	0.812		Measured DSD (OK), Bringi's shape	NSSL
6	47.3	0.791		Measured DSD (OK), Brandes' shape	NSSL
$R(Z, Z_{DR}) = a Z^b Z_{DR}^c$					
	a	b	c	Assumptions	Source
7	6.70×10^{-3}	0.927	-3.43	Simulated DSD, equilibrium shape	BC01
8	7.46×10^{-3}	0.945	-4.76	Measured DSD (FL), Brandes' shape	BZV02
9	7.11×10^{-3}	1.0	*	Simulated DSD, Goddard's shape	IB02
10	1.42×10^{-2}	0.770	-1.67	Measured DSD (OK), equilibrium shape	NSSL
11	1.59×10^{-2}	0.737	-1.03	Measured DSD (OK), Bringi's shape	NSSL
12	1.44×10^{-2}	0.761	-1.51	Measured DSD (OK), Brandes' shape	NSSL
$R(K_{DP}, Z_{DR}) = a K_{DP} ^b Z_{DR}^c \text{sign}(K_{DP})$					
	a	b	c	Assumptions	Source
13	90.8	0.93	-1.69	Simulated DSD, equilibrium shape	BC01
14	136	0.968	-2.86	Measured DSD (FL), Brandes' shape	BZV02
15	52.9	0.852	-0.53	Measured DSD (OK), equilibrium shape	NSSL
16	63.3	0.851	-0.72	Measured DSD (OK), Bringi's shape	NSSL

* Here, $c = -8.14 + 1.385Z_{DR} - 0.1039Z_{DR}^2$.

performed in order to obtain point estimates of hourly rain total:

- 1) The estimates of Z and K_{DP} are converted into rain rates $R(Z)$ and $R(K_{DP})$ for each range gate using Eq. (1) and relation 4 from Table 1.
- 2) The ρ_{hv} threshold of 0.85 is used to eliminate the echoes of nonmeteorological origin (ground clutter, anomalous propagation, biological scatterers, chaff, etc.). In all gates with nonmeteorological echoes $R(Z)$, $R(K_{DP})$, and Z_{DR} are set to zero.
- 3) The estimates of $R(Z)$, $R(K_{DP})$, and Z_{DR} are averaged over two radials and five range gates closest to a particular gauge to obtain mean values $\overline{R(Z)}$, $\overline{R(K_{DP})}$, and $\overline{Z_{DR}}$ for an area of about $1 \text{ km} \times 1^\circ$ that is centered on the gauge. Averaging rain rates rather than Z and K_{DP} is dictated by nonlinearity of the $R(Z)$ and $R(K_{DP})$ relations.
- 4) Mean values \overline{Z} and $\overline{K_{DP}}$ are obtained by inverting $\overline{R(Z)}$ and $\overline{R(K_{DP})}$.
- 5) Rain rates corresponding to the $1 \text{ km} \times 1^\circ$ spatial domain are computed using mean values of Z , Z_{DR} , and K_{DP} , and the algorithms listed in Table 1.
- 6) One-hour accumulations for different rainfall relations are obtained via summing up the corresponding rain-rate estimates.

Note that instead of spatially averaging the $R(Z, Z_{DR})$ and $R(K_{DP}, Z_{DR})$ estimates in individual gates, we use the spatially averaged values \overline{Z} , $\overline{K_{DP}}$, and $\overline{Z_{DR}}$ to compute rain rates assigned to the $1 \text{ km} \times 1^\circ$ area. This allows us to reduce the impact of the "measure-

ment noise" in the raw K_{DP} and Z_{DR} data on the quality of rain estimates. Further reduction of statistical errors is achieved after rain rates are summed up to obtain hourly rain totals. Update times for rain-rate estimates were different for rain events observed in 2002 and 2003. In 2002, volume coverage pattern (VCP) included only the two lowest elevation tilts— 0.5° and 1.5° —whereas in 2003 the VCP consisting of 14–15 elevation angles was implemented. Thus, the update times for rain-rate estimates were about 2 and 6 min in 2002 and 2003, respectively. Only the data collected at elevation 0.5° were used for rainfall estimation.

4. Validation and optimization of polarimetric rainfall algorithms using the ARS Micronet gauges

To characterize the quality of different polarimetric rain algorithms, we examine a fractional bias (FB)

$$\text{FB} = \frac{\langle T_R - T_G \rangle}{\langle T_G \rangle}, \quad (6)$$

fractional rms error (FRMSE)

$$\text{FRMSE} = \frac{\langle (T_R - T_G)^2 \rangle^{1/2}}{\langle T_G \rangle}, \quad (7)$$

and fractional standard deviation (FSD) of rainfall estimates

$$\text{FSD} = (\text{FRMSE}^2 - \text{FB}^2)^{1/2}, \quad (8)$$

where T_R and T_G are radar and gauge hourly totals for any given radar–gauge pair and brackets mean averaging over all such pairs.

a. Statistical properties of different rainfall estimates

Fractional biases, standard deviations, and rms errors of the point and areal radar-rainfall estimates for the conventional and various polarimetric relations listed in Table 1 are summarized in Table 2. The number of radar–gauge pairs that were used to compute statistical parameters in Table 2 is 1813 for hourly point rainfall estimates. The number of areal mean rain rates is 50. The average hourly gauge accumulation is 6.3 mm for the whole dataset.

There is an obvious overall improvement in rainfall estimation when we switch from $R(Z)$ to any polarimetric algorithm. This improvement is also illustrated by Figs. 3 and 4 where the radar–gauge scatterplots are shown for the conventional algorithm and three polarimetric algorithms that perform the best in terms of the rms error for each of the $R(K_{\text{DP}})$, $R(Z, Z_{\text{DR}})$, and $R(K_{\text{DP}}, Z_{\text{DR}})$ categories (algorithms 4, 10, and 14 in Table 1, respectively). It is evident that the conventional algorithm tends to overestimate rain for this dataset, most likely due to the presence of hail in many

storms observed during the spring and summer of 2003. The use of the $R(K_{\text{DP}})$ relation results in an apparent reduction of the bias and rms error when compared with $R(Z)$. Further improvement, although not as dramatic, is achieved if the two-parameter polarimetric algorithms are utilized.

Generally, polarimetric estimates of rain are less susceptible to the DSD variations than the standard $R(Z)$ relation. However, they are more prone to statistical measurement errors of polarimetric variables than are the $R(Z)$ estimates to statistical errors in Z . Part of the scatter in Figs. 3b, 3c, and 3d is attributed to such “measurement noise” that is considerably reduced in areal rainfall estimates (the corresponding panels in Fig. 4). The $R(K_{\text{DP}}, Z_{\text{DR}})$ algorithm demonstrates the most impressive improvement for areal mean rain rates exceeding 5 mm h^{-1} , whereas the $R(Z, Z_{\text{DR}})$ relation performs better than others at lower rain rates.

b. A “synthetic” rainfall algorithm

An ultimate goal of this study is to find an optimal rainfall algorithm that works best of all for the JPOLE dataset. Can we do better than the best of the algorithms listed in Table 1? Intuitively, it is obvious that using different combinations of radar variables for different categories of rain intensity might be beneficial (Chandrasekar et al. 1993). If the rms error is used as a quality criterion, then the joint use of Z and Z_{DR} is advantageous for point measurements of rain, whereas the combination of K_{DP} and Z_{DR} is a preferable choice for areal estimates.

The coefficients in the $R(Z, Z_{\text{DR}})$ and $R(K_{\text{DP}}, Z_{\text{DR}})$ relations depend on the statistics of DSD and raindrop shapes. Direct measurements of drop shapes with a 2D video disdrometer remain problematic (Ryzhkov and Schuur 2003). An alternative radar method for raindrop shape retrieval was suggested by Gorgucci et al. (2000). According to this method, a linear dependence of the axis ratio on equivolume raindrop diameter is assumed, and the slope of such dependence is obtained from the measured Z , Z_{DR} , and K_{DP} . This method, however, is still in a developing stage and was not tested on a large dataset. The assumption about linear dependence of raindrop oblateness on its diameter might be too simplistic.

In other words, the prevalent shape of raindrops in the observed rain events is unknown and represents serious uncertainty. Instead of speculating about actual drop shape, we resort to a semiempirical approach to obtain “optimal” $R(Z, Z_{\text{DR}})$ and $R(K_{\text{DP}}, Z_{\text{DR}})$ relations. According to such an approach, the ratios of mean areal rain rates from the radar $\langle R \rangle$ and gauges $\langle G \rangle$ are examined as functions of a “net” Z_{DR} , provided that the one-parameter $R(Z)$ and $R(K_{\text{DP}})$ relations are utilized. The net value of differential reflectivity $\langle Z_{\text{DR}} \rangle$ is defined as a weighted average Z_{DR} for a particular hour over a whole gauge network:

TABLE 2. Fractional mean biases, fractional standard deviations, and fractional rms errors of the radar estimates of 1-h rain totals and areal mean rain rates (%) for different radar-rainfall algorithms listed in Table 1.

Algorithm	Point			Areal	
	FB (%)	FSD (%)	FRMSE (%)	FSD (%)	FRMSE (%)
$R(Z) = 1.70 \times 10^{-2} Z^{0.714}$					
	19.4	82.0	84.2	60.1	64.6
$R(K_{\text{DP}}) = a K_{\text{DP}} ^b \text{sign}(K_{\text{DP}})$					
1	1.1	69.4	69.4	45.0	45.0
2	12.1	75.5	76.4	50.7	52.5
3	16.0	69.3	71.2	44.3	47.7
4	−10.3	58.0	58.9	32.9	34.2
5	3.3	67.8	68.0	43.4	43.7
6	−1.1	62.4	62.6	37.9	37.9
$R(Z, Z_{\text{DR}}) = a Z^b Z_{\text{DR}}^c$					
7	17.8	70.5	72.8	39.8	44.2
8	3.5	62.9	62.9	26.5	26.8
9	12.4	72.9	74.0	35.2	37.7
10	−5.1	50.0	50.2	26.0	26.2
11	−4.1	52.7	52.9	29.9	29.9
12	−6.7	50.0	50.5	26.0	26.5
$R(K_{\text{DP}}, Z_{\text{DR}}) = a K_{\text{DP}} ^b Z_{\text{DR}}^c \text{sign}(K_{\text{DP}})$					
13	−9.1	52.9	53.7	25.4	26.7
14	−11.0	54.6	55.8	21.7	24.2
15	−14.0	52.7	54.6	27.0	30.0
16	−4.0	56.9	57.0	32.0	32.1

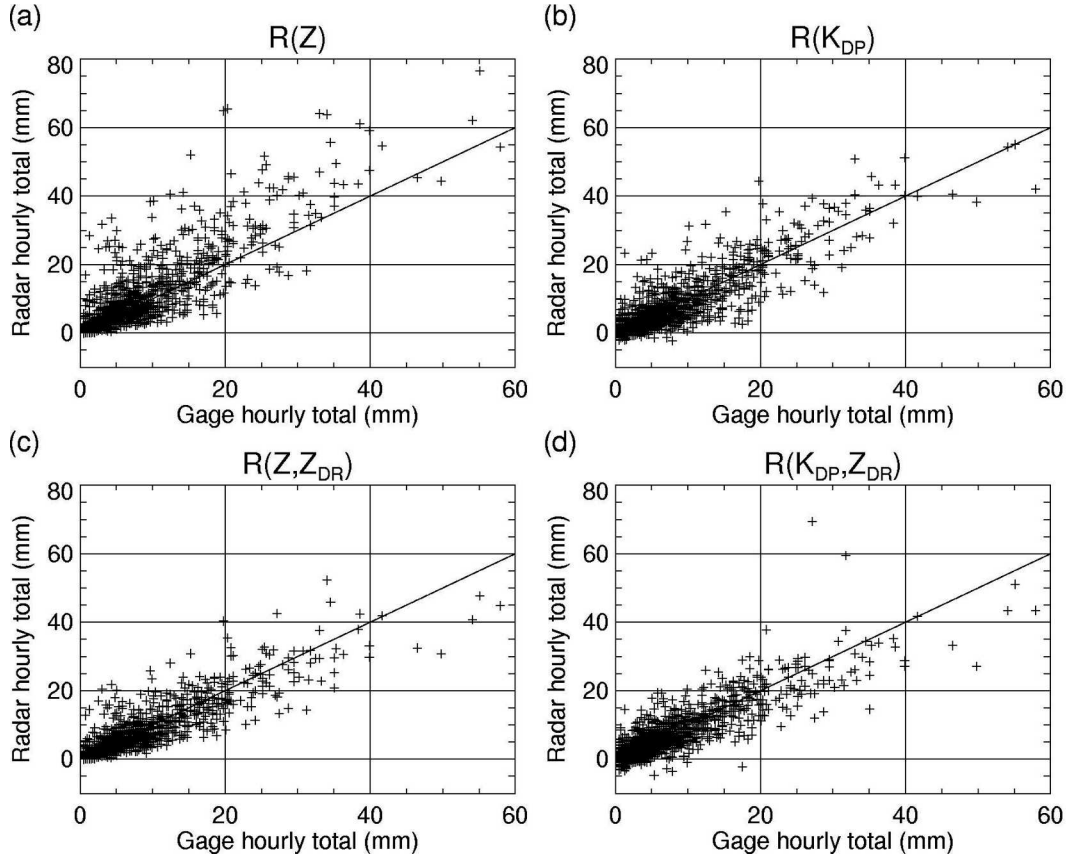


FIG. 3. One-hour individual gauge rain accumulations vs their estimates from different radar-rainfall algorithms (24 rain events, 50 h of observations). The $R(K_{DP})$, $R(Z, Z_{DR})$, and $R(K_{DP}, Z_{DR})$ relations are the best in each category (algorithms 4, 10, and 14 in Table 1, respectively).

$$\langle Z_{DR} \rangle = \frac{\sum_{i,j} R^{i,j}(Z) Z_{DR}^{i,j}}{\sum_{i,j} R^{i,j}(Z)}, \quad (9)$$

where superscript i characterizes the scan number within the 1-h time interval and superscript j stands for the gauge number. Because differential reflectivities that are associated with larger rain rates are more important to characterize rain regime and its impact on the total rain estimation than the ones associated with light rain, each Z_{DR} measurement is weighted proportionally to the rain rate computed from the $R(Z)$ relation. Thus, the net Z_{DR} characterizes the most intense part of rain for a given hour in the gauge area.

Figure 5 shows scattergrams of $\langle R(Z) \rangle / \langle G \rangle$ and $\langle R(K_{DP}) \rangle / \langle G \rangle$ versus $\langle Z_{DR} \rangle$ for 50 h of observations. Mean areal rain rates $\langle R(Z) \rangle$ and $\langle R(K_{DP}) \rangle$ are computed using Eq. (1) and algorithm 4 from Table 1:

$$R(K_{DP}) = 44.0 |K_{DP}|^{0.822} \text{sign}(K_{DP}). \quad (10)$$

It is quite clear from Fig. 5 that both $R(Z)$ and $R(K_{DP})$ tend to underestimate rain in which DSD is dominated by smaller drops (low $\langle Z_{DR} \rangle$) and overesti-

mate it if rain is characterized with a large raindrop median diameter (high $\langle Z_{DR} \rangle$). If the net Z_{DR} values are less than 1 dB, the K_{DP} -based algorithm produces larger negative bias than the conventional one. For a warm season convective rain with high Z_{DR} , the $R(K_{DP})$ estimate is much less sensitive to the median raindrop diameter than its conventional counterpart.

The observed dependencies of $\langle R(Z) \rangle / \langle G \rangle$ and $\langle R(K_{DP}) \rangle / \langle G \rangle$ on $\langle Z_{DR} \rangle$ have a simple physical explanation. As was pointed out by Ryzhkov and Znic (1996), for larger drop sizes $K_{DP} \sim D^{4.24}$, whereas for smaller drop sizes $K_{DP} \sim D^{5.6}$ (where D is an equivolume raindrop diameter). The rain rate is approximately proportional to the 3.67th moment of the DSD. Therefore, at lower rain rates mostly associated with smaller drops, the $R(K_{DP})$ relation is more susceptible to the variations in the DSD than at higher rain rates.

The ratio $\langle R(K_{DP}) \rangle / \langle G \rangle$ exhibits noticeably tighter dependence (less scatter) on the net differential reflectivity than the ratio $\langle R(Z) \rangle / \langle G \rangle$. This means that we may achieve better success in eliminating a dependency of results for rain estimation on the median drop diameter (or DSD variations) if the K_{DP} - Z_{DR} pair is selected.

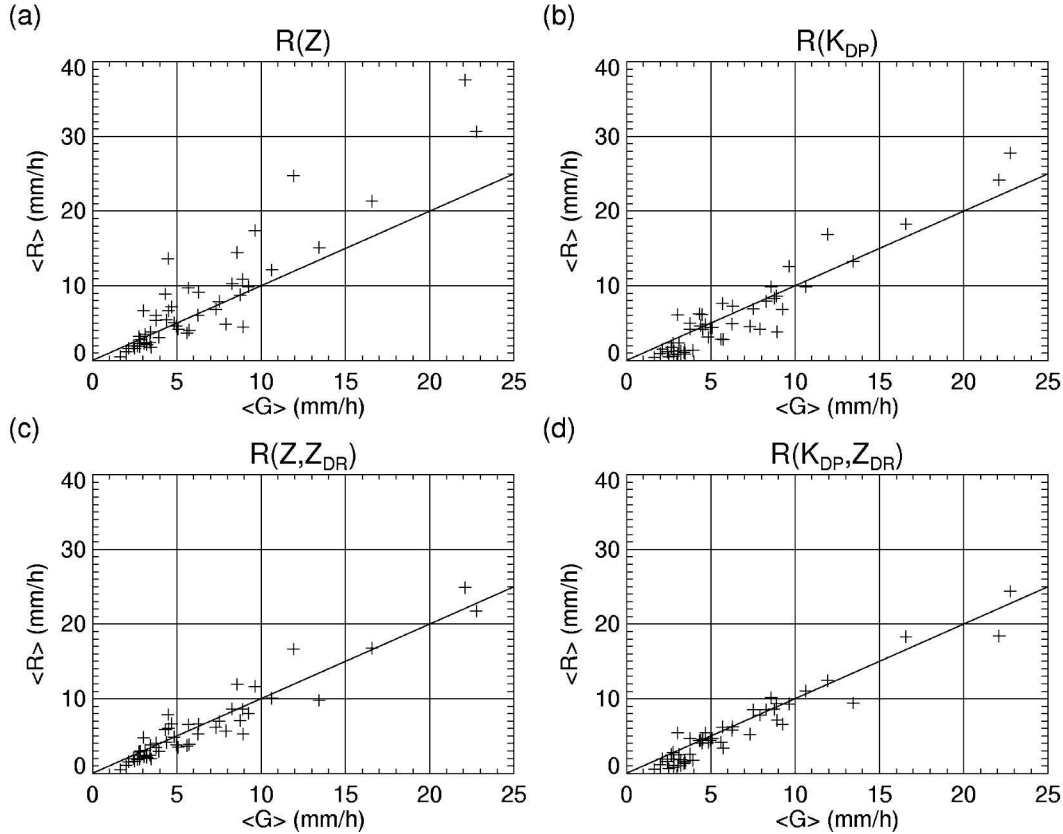


FIG. 4. Mean areal rain rates from gauges $\langle G \rangle$ vs their estimates $\langle R \rangle$ from different radar-rainfall algorithms (24 rain events, 50 h of observations). The $R(K_{DP})$, $R(Z, Z_{DR})$, and $R(K_{DP}, Z_{DR})$ relations are the best in each category (algorithms 4, 10, and 14 in Table 1, respectively).

Similar conclusions can be drawn from Fig. 6 where the net Z_{DR} , as well as the ratios of the mean areal rain rates obtained from the radar and gauges are displayed versus an hour of observations ranked in chronological order. Rain overestimation associated with large $\langle Z_{DR} \rangle$ in the 2003 spring season (hours 32–40) is much more pronounced for the $R(Z)$ algorithm than for the $R(K_{DP})$ relation. In the case of heavy rain associated with large hail on 14 May 2003 ($x = 36$ in Fig. 6), $\langle R(Z) \rangle / \langle G \rangle = 3.1$, whereas $\langle R(K_{DP}) \rangle / \langle G \rangle = 1.4$.

Following an approach by Fulton et al. (1999), we used the data displayed in Fig. 5 to approximate mean dependencies $\langle R \rangle / \langle G \rangle = f(\langle Z_{DR} \rangle)$ with relatively simple functions:

$$\langle R(Z) \rangle / \langle G \rangle = f_1(\langle Z_{dr} \rangle) = 0.4 + 5.0|\langle Z_{dr} \rangle - 1|^{1.3}, \quad (11)$$

and

$$\langle R(K_{DP}) \rangle / \langle G \rangle = f_2(\langle Z_{dr} \rangle) = 0.4 + 3.5|\langle Z_{dr} \rangle - 1|^{1.7}, \quad (12)$$

where $\langle Z_{dr} \rangle$ is the net differential reflectivity expressed in linear units [$\langle Z_{dr} \rangle = 10^{0.1\langle Z_{DR} \rangle(\text{dB})}$]. Relations (11) and (12) were used to build a “composite” or “synthetic” $R(Z, K_{DP}, Z_{DR})$ algorithm that capitalizes on the rela-

tive merits of the $R(Z, Z_{DR})$, $R(K_{DP}, Z_{DR})$, and $R(K_{DP})$ relations for different categories of rain intensity. The following is a description of the proposed algorithm:

$$R = \overline{R(Z)} / f_1(\overline{Z_{dr}}) \text{ if } \overline{R(Z)} < 6 \text{ mm h}^{-1}, \quad (13)$$

$$R = \overline{R(K_{DP})} / f_2(\overline{Z_{dr}}) \text{ if } 6 < \overline{R(Z)} < 50 \text{ mm h}^{-1}, \quad (14)$$

and

$$R = \overline{R(K_{DP})} \text{ if } \overline{R(Z)} > 50 \text{ mm h}^{-1}, \quad (15)$$

where relations $R(Z)$, $R(K_{DP})$, and functions $f_{1,2}$ are determined by (1), (10), (11), and (12), respectively. Note that mean values $\overline{R(Z)}$, $\overline{R(K_{DP})}$, and $\overline{Z_{dr}}$ are obtained after averaging over the $1 \text{ km} \times 1^\circ$ area, as explained in section 3.

The $R(Z, K_{DP}, Z_{DR})$ algorithm is structured in such a way that the combination of K_{DP} and Z_{DR} is used for estimation of about one-half of all rainfall in Oklahoma according to the DSD statistics. It is known from simulations that, when compared with the $R(Z)$, $R(K_{DP})$, and $R(Z, Z_{DR})$ relations, the $R(K_{DP}, Z_{DR})$ algorithm is least affected by DSD variations and uncertainties in raindrop shapes and canting. At lower rain rates ($< 6 \text{ mm h}^{-1}$), the combination of K_{DP} and Z_{DR} is less effi-

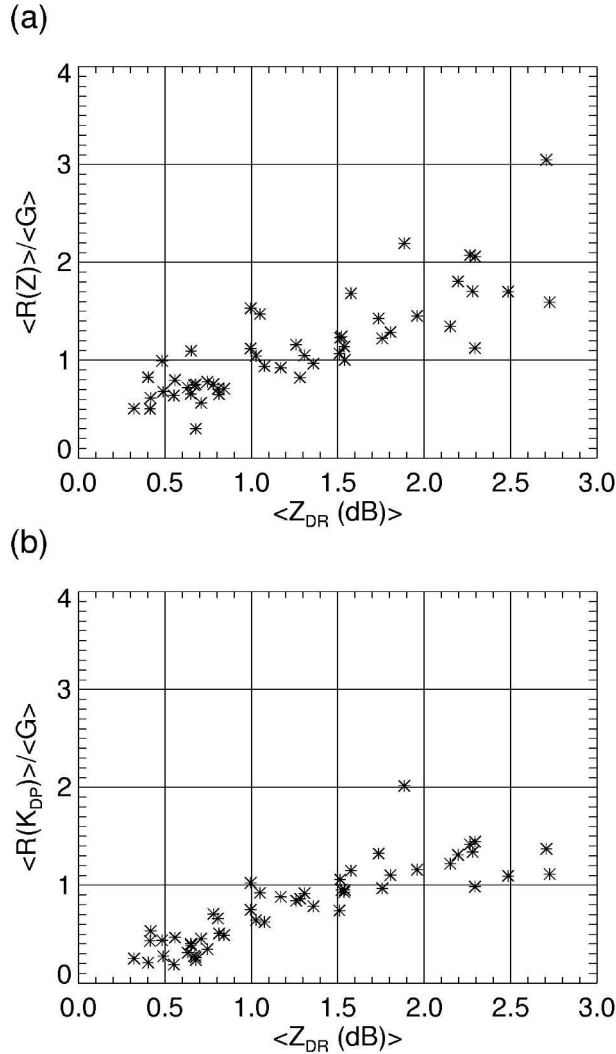


FIG. 5. Scatterplots of the ratios of mean areal rain rates obtained from radar and gauges vs net values of differential reflectivity for the $R(Z)$ and $R(K_{DP})$ algorithms.

cient because K_{DP} becomes too noisy. Therefore, Z (instead of K_{DP}) should be used jointly with Z_{DR} . For very high rain rates ($>50 \text{ mm h}^{-1}$), both Z_{DR} and Z are very likely contaminated with hail, and the synthetic algorithm relies exclusively on K_{DP} .

According to the synthetic algorithm, reflectivity calibration is required only for estimation of light rain with intensity less than 6 mm h^{-1} (which accounts for about 32% of the annual rain in Oklahoma) and for determining the choice among Eqs. (13)–(15). Thus, the issue of accurate absolute calibration of Z is less critical for successful performance of the synthetic algorithm than of the conventional method that is solely based on Z .

Although the functions f_1 and f_2 were originally determined at a large scale for mean areal rain rates and net differential reflectivities (i.e., the $40 \text{ km} \times 30 \text{ km}$

area and 1-h integration), we recommend applying the same functions at a smaller scale ($1 \text{ km} \times 1^\circ$ spatial resolution for each individual scan). The choice of Z_{dr} (in linear scale) instead of \overline{Z}_{DR} (in logarithmic scale) in Eqs. (13)–(14) is dictated by the need to reduce the impact of statistical measurement errors in differential reflectivity at a smaller scale.

c. The performance of the synthetic algorithm

The coefficients in Eqs. (11) and (12) determining the synthetic algorithm were originally obtained using a subset of rain events observed in 2002. Then the algorithm was tested using the whole dataset containing all rain events in 2002 and 2003 for which the ARS and Mesonet data were available. Very little tuning of the coefficients was required to optimize the algorithm for the whole JPOLE dataset.

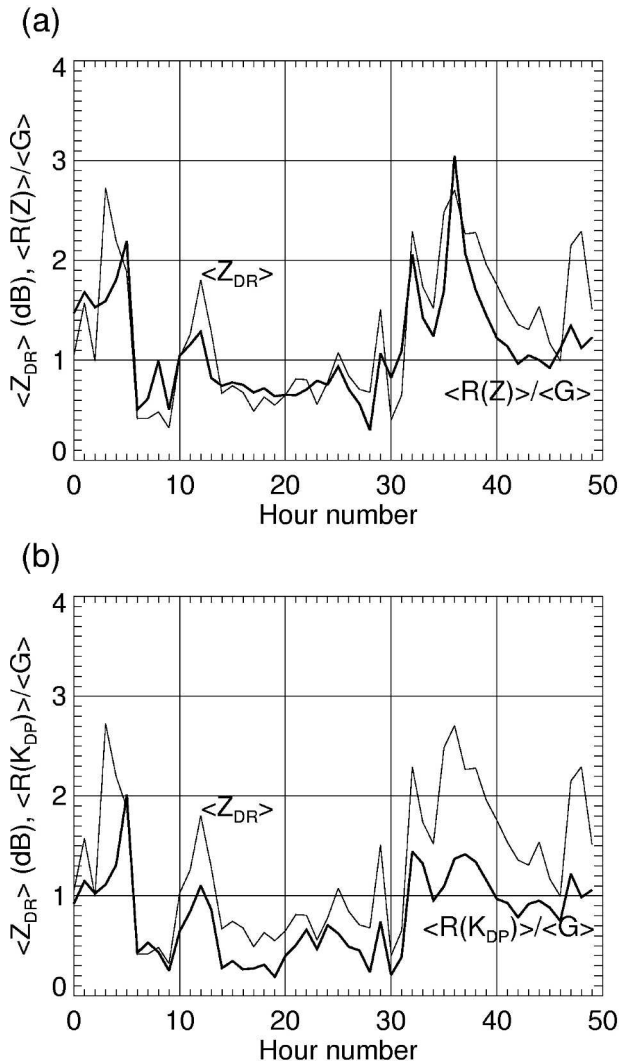


FIG. 6. Net Z_{DR} and ratios of mean areal rain rates from radar vs hour of observations ranked in chronological order.

TABLE 3. Fractional mean biases, fractional standard deviations, and fractional rms errors of the radar estimates of 1-h rain totals and areal mean rain rates (%) for the best radar-rainfall algorithms in each category.

Algorithms	Point			Areal	
	FB (%)	FSD (%)	FRMSE (%)	FSD (%)	FRMSE (%)
$R(Z)$	19.4	82.0	84.2	60.1	64.6
$R(K_{DP})$	-10.3	58.0	58.9	32.9	34.2
$R(Z, Z_{DR})$	-5.1	50.0	50.2	26.0	26.2
$R(K_{DP}, Z_{DR})$	-11.0	54.6	55.8	21.7	24.2
$R(Z, K_{DP}, Z_{DR})$	-0.2	48.6	48.6	17.5	17.5

The $R(Z, K_{DP}, Z_{DR})$ algorithm outperforms all of the others according to all five statistical criteria: it has the lowest bias, standard deviations, and rms errors for point and areal rainfall estimates (Table 3). Figure 7 shows scatterplots of hourly totals obtained from the $R(Z)$ and $R(Z, K_{DP}, Z_{DR})$ relations versus 1-h gauge accumulations for individual radar-gauge comparisons and areal estimates. The synthetic polarimetric algorithm has very small overall bias and demonstrates a significant reduction of the rms errors when compared with

the conventional rainfall estimator—1.7 times for point measurements and 3.7 times for areal rainfall estimates.

Fractional biases FB and standard errors FRMSE of rainfall estimates are inversely proportional to the mean rain total $\langle T_G \rangle$. Fractional rms errors are higher for lower rain accumulations. Table 4 summarizes the estimates of FB and FRMSE for different algorithms in the three categories of hourly rain totals: low ($T_G < 5$ mm), medium ($5 < T_G < 30$ mm), and high ($T_G > 30$ mm). The synthetic algorithm outperforms others in all three categories. However, it tends to overestimate light rain and underestimate heavy rain. The fractional bias is smallest for moderate rain.

In addition to the conventional NEXRAD relation $Z = 300R^{1.4}$, we also examined the performance of two other $R(Z)$ relations: $Z = 303R^{1.44}$ and $Z = 527R^{1.41}$. The first is matched with the observed 25 920 DSDs, whereas the second yields the smallest fractional rms errors among all possible power-law $R(Z)$ relations for the JPOLE dataset (64.3% and 41.6% for point and areal estimates, respectively). Note that even the performance of this optimal $R(Z)$ algorithm is not as good as other polarimetric algorithms from Table 3. The “disdrometer matched” relation $Z = 303R^{1.44}$ gives the

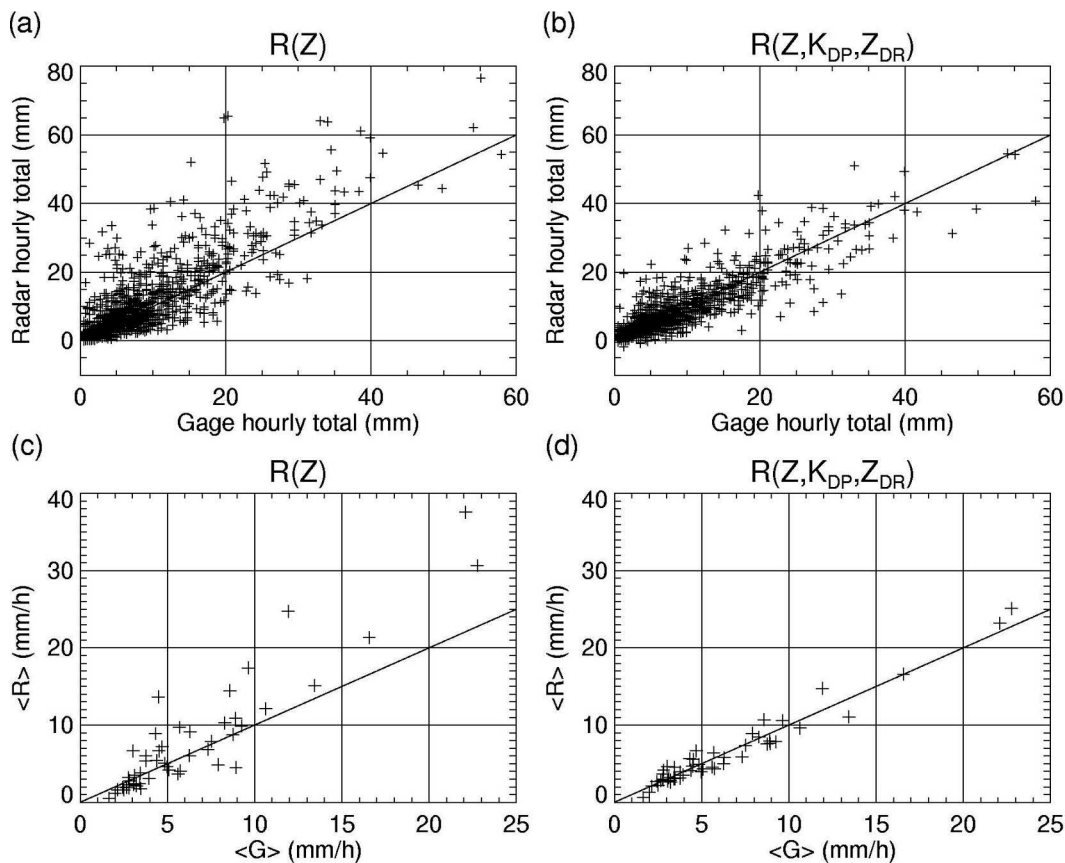


FIG. 7. One-hour (top) accumulations and (bottom) mean areal rain rates from gauges vs their estimates from the $R(Z)$ and $R(Z, K_{DP}, Z_{DR})$ algorithms (24 rain events, 50 h of observations).

TABLE 4. Fractional mean biases and fractional rms errors of the radar estimates of 1-h rain totals (%) for different algorithms in the three categories of hourly rain totals: low ($T_G < 5$ mm), medium ($5 < T_G < 30$ mm), and high ($T_G > 30$ mm).

Algorithm	FB (%)			FRMSE (%)		
	Low	Medium	High	Low	Medium	High
$R(Z)$	19.3	18.9	23.2	119.6	66.7	35.7
$R(K_{DP})$	-23.9	-7.0	-0.3	95.7	45.9	20.4
$R(Z, Z_{DR})$	2.5	-6.7	-13.2	73.7	38.3	25.4
$R(K_{DP}, Z_{DR})$	-18.5	-7.8	-15.7	85.0	41.8	28.8
$R(Z, K_{DP}, Z_{DR})$	14.4	-4.2	-7.3	68.4	38.2	22.0

fractional rms errors 73.2% and 53.1% for point and areal measurements, respectively, that is, between the ones from the standard and optimal $R(Z)$ relations.

Figure 8 shows the bias in areal rain rates that are estimated from radar using the $R(Z, K_{DP}, Z_{DR})$ and two $R(Z)$ relations versus hour of observations ranked in chronological order. The three curves in Fig. 8 illustrate the overall overestimation/underestimation of rain with three algorithms for different seasons and rain regimes. As was already mentioned, the conventional $R(Z)$ algorithm tends to significantly overestimate rainfall associated with intense convection, and especially with hail reported for many spring events (Heinselman and Ryzhkov 2004). The polarimetric method suggested by Eqs. (13)–(15) dramatically reduces such overestimation. Both methods slightly underestimate rain for cold season stratiform events with marginal improvement if the polarimetric algorithm is used (hours 10–30, October/December 2002). The optimal $R(Z)$ relation produces a smaller positive bias for warm season rain events and a significantly larger negative bias for cold season events than the standard WSR-88D relation. In other words, application of the optimal $R(Z)$ relation shifts the thin solid curve, illustrating the performance of the standard $R(Z)$ algorithm downward, without much change in its shape. There is not a single $R(Z)$ relation that matches well the observed rain regimes,

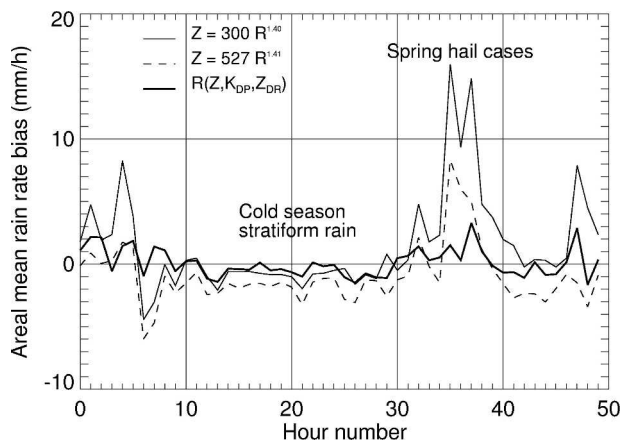


FIG. 8. The bias in areal rain rates estimated from radar using the $R(Z)$ and $R(Z, K_{DP}, Z_{DR})$ algorithms vs hour of observations ranked in chronological order.

whereas the polarimetric algorithm automatically accounts for the differences between various types of rain.

It is evident from Fig. 8 that the overall statistical properties of different rainfall estimators are heavily weighted by convective precipitation during the warm season, and the majority of the improvement due to application of dual polarization is attributed to heavy convective precipitation. We do not exclude the possibility that, in different geographical areas where rain originated from hail is less likely than in Oklahoma, the use of polarimetric rain measurements may not lead to such remarkable and indisputable improvement as in the U.S. Great Plains, which are notorious for severe weather.

Figure 9 gives graphical representation of the relative performance of different types of rainfall estimators if the point, and areal rms errors are used as criteria. The biggest reduction in the rms errors is achieved after switching from the $R(Z)$ algorithm to the $R(K_{DP})$ estimator. Further optimization of the dual-polarization algorithm (adding Z_{DR}) results in additional improvement, although not as dramatic as during the first step. Additional sophistication of the polarimetric algorithm yields better payoff in the areal rainfall estimation. The transition from the $R(K_{DP})$ algorithm to the $R(Z, K_{DP}, Z_{DR})$

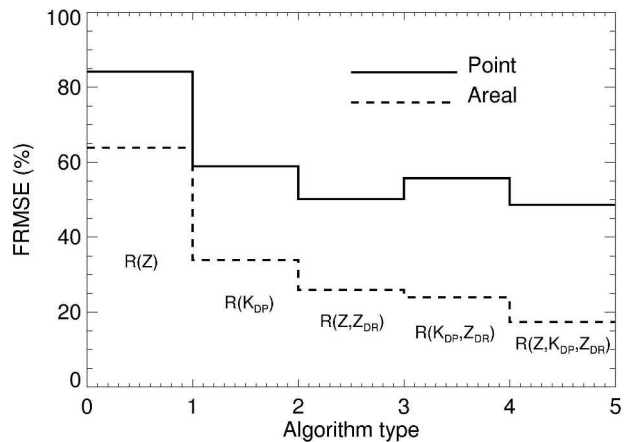


FIG. 9. Fractional rms errors of point and areal estimates of rain for different radar-rainfall algorithms. The $R(K_{DP})$, $R(Z, Z_{DR})$, and $R(K_{DP}, Z_{DR})$ relations are the best in each category (algorithms 4, 10, and 14 in Table 1, respectively).

Z_{DR}) relation leads to a 2 times reduction of the rms error of the areal rain estimate. The corresponding improvement in point estimates is more modest. Note that the $R(Z, Z_{DR})$ algorithm outperforms the $R(K_{DP}, Z_{DR})$ estimator for point measurements, but the opposite is true for areal estimates. This is additional confirmation of the fact the K_{DP} -based algorithms are better suited for bigger watershed areas.

5. Evidence of different rain regimes

A large variety of rain regimes that is characterized by different types of DSD was encountered during JPOLE. The $Z-Z_{DR}$ scattergrams give insight into microphysical properties of rain and the type of DSDs associated with these regimes. For a given Z , very large values of Z_{DR} generally indicate DSDs that are skewed toward bigger drops, whereas very small values of Z_{DR} suggest a dominance of small drops. The slope of the $Z-Z_{DR}$ scattergram and its spread are good predictors of rainfall overestimation/underestimation if the $R(Z)$ relation is used.

Quite often two distinct clusters of the $Z-Z_{DR}$ pairs are evident in the scattergrams (see Fig. 10, e.g.). This happens most frequently in stratiform rain with weak embedded convection. Raindrops in the stratiform part of the storm usually originate from big snowflakes in the melting layer, whereas the weak convective cells are dominated by drops produced from smaller-sized graupel. Therefore, weak convective elements are characterized by smaller values of Z_{DR} for the same Z when compared with their stratiform counterparts. For strong convection, the opposite is true.

The top panels in Fig. 10 demonstrate the $Z-Z_{DR}$ scattergrams obtained from the data in the $50 \text{ km} \times 40 \text{ km}$ area encompassing the ARS gauges (Fig. 1) for two stratiform rain events with embedded convection observed on 9 September 2002 (left top panel) and 9 October 2002 (right top panel). These scattergrams summarize 1 h of data collected with $1 \text{ km} \times 1 \text{ km}$ resolution at the elevation of 0.5° . The $Z-Z_{DR}$ clusters with lower Z_{DR} and higher maximal Z in both panels are associated with relatively weak embedded convection.

As the rest of the panels in Fig. 10 show, the highest hourly gauge totals corresponding to rain from convective elements are significantly underestimated by the radar, whereas the smaller rain totals associated with pure stratiform precipitation are measured more accurately. Such underestimation is especially pronounced for the NEXRAD $R(Z)$ relation. There is no way for any single $R(Z)$ relation that is not sensitive to microphysical differences to “match” both rain regimes in a relatively small spatial/temporal domain. The polarimetric method automatically accounts for microphysical distinctions between the two rain types and, therefore, yields more accurate estimates of rain (bottom panels in Fig. 10). It should be admitted, however, that

the highest hourly totals in both cases remain underestimated (although to a lesser degree) even after the “synthetic” algorithm is applied.

Another two examples with very different types of DSD are illustrated in Fig. 11. The rain event on 8 September 2002 (Fig. 11, left side) was associated with a tropical air mass. This case is characterized by very “flat” $Z-Z_{DR}$ scattergrams and pronounced underestimation of rainfall if the conventional $R(Z)$ algorithm is used. It is interesting that the observed values of Z_{DR} barely exceed 1 dB, even for reflectivities reaching 50 dBZ.

In the second example, the storm on 14 May 2003 (Fig. 11, right side) produced intense rainfall (near-flash-flood criteria) in the ARS Micronet area and hail with sizes exceeding 13 cm. Some of the Micronet gauges recorded rain rates of about 200 mm h^{-1} and at least three gauges registered hourly rain totals exceeding 50 mm. The sharp decrease of Z_{DR} for $Z > 60 \text{ dBZ}$ is a clear indication of hail. Hail cores are typically surrounded by regions of very high Z_{DR} that can be attributed to melting hail or giant raindrops with ice cores inside. The contribution of such areas to rain total usually is much larger than the contribution from “pure” hail-contaminated regions where high Z is coupled with low Z_{DR} .

The $Z-Z_{DR}$ scattergrams for rain mixed with hail are extremely broad, that is, very high values of Z_{DR} are observed in a wide range of reflectivities, including very low ones. This explains why thresholding Z at certain level (53 dBZ for the WSR-88D radars) only partially mitigates the impact of hail on the quality of rain measurement. We still observe substantial overestimation of rain after the 53-dBZ threshold is applied to the radar reflectivity data (Fig. 11).

Application of the polarimetric method results in significant improvement in both cases; the overall biases are almost eliminated (Fig. 11, bottom panels), that is, the mean areal rain rates from the radar and gauges agree very well. The width of the scattergram for the hail case, however, remains quite significant for both estimates. This might point to additional sampling problems that have a larger impact on the K_{DP} -based rainfall algorithms because of large measurement errors of K_{DP} . Although we do not observe systematic deterioration in polarimetric rain estimation for the 2003 rain events, sampled with an update time of 6 min (as opposed to the 2002 events with 3 times faster update), nonetheless, cursory examination of isolated convection suggests that more frequent sampling might be beneficial for the application of the synthetic polarimetric algorithm.

According to the existing NEXRAD scanning strategy (Crum et al. 1993), the azimuthal sweep at the lowest two elevation angles (0.5° and 1.5°) is repeated to permit one sweep in a surveillance mode (to map the reflectivity field) and another in a Doppler mode (to measure radial velocities while mitigating range fold-

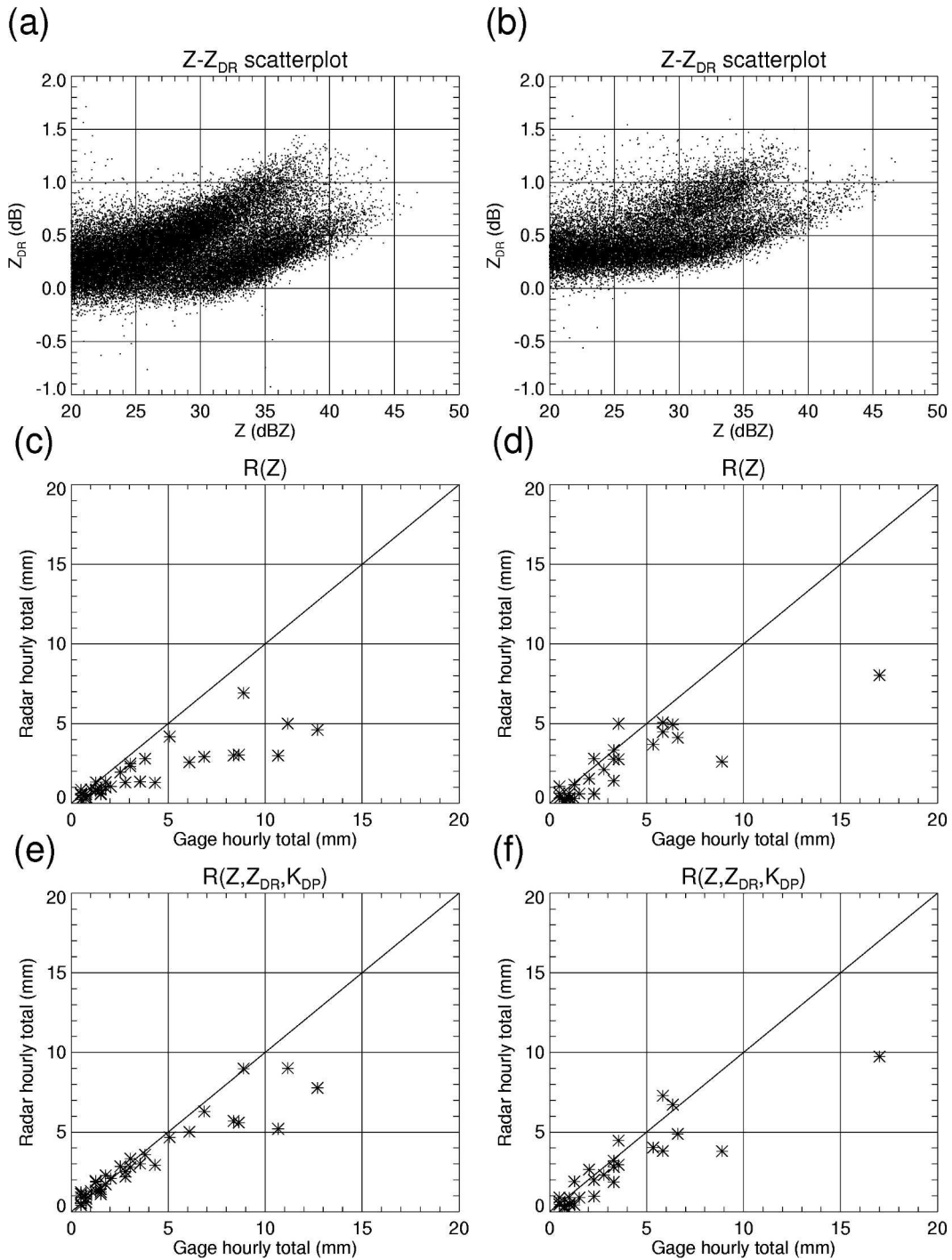


FIG. 10. $Z-Z_{DR}$ scattergrams and hourly ARS gauge totals vs rainfall estimates from the $R(Z)$ and $R(Z, K_{DP}, Z_{DR})$ algorithms for two cases of stratiform rain with embedded convection: (left) 1600–1700 UTC 9 Sep 2002 and (right) 1300–1400 UTC 9 Oct 2002.

ing, performing velocity dealiasing, and suppressing ground clutter). Making polarimetric measurements at the two successive sweeps would reduce the “sampling” and “instrumental” noise in polarimetric rainfall estimates.

6. Conclusions

The rain measurement capability of the polarimetric prototype of WSR-88D with simultaneous transmission and a short dwell time has been tested using a large dataset.

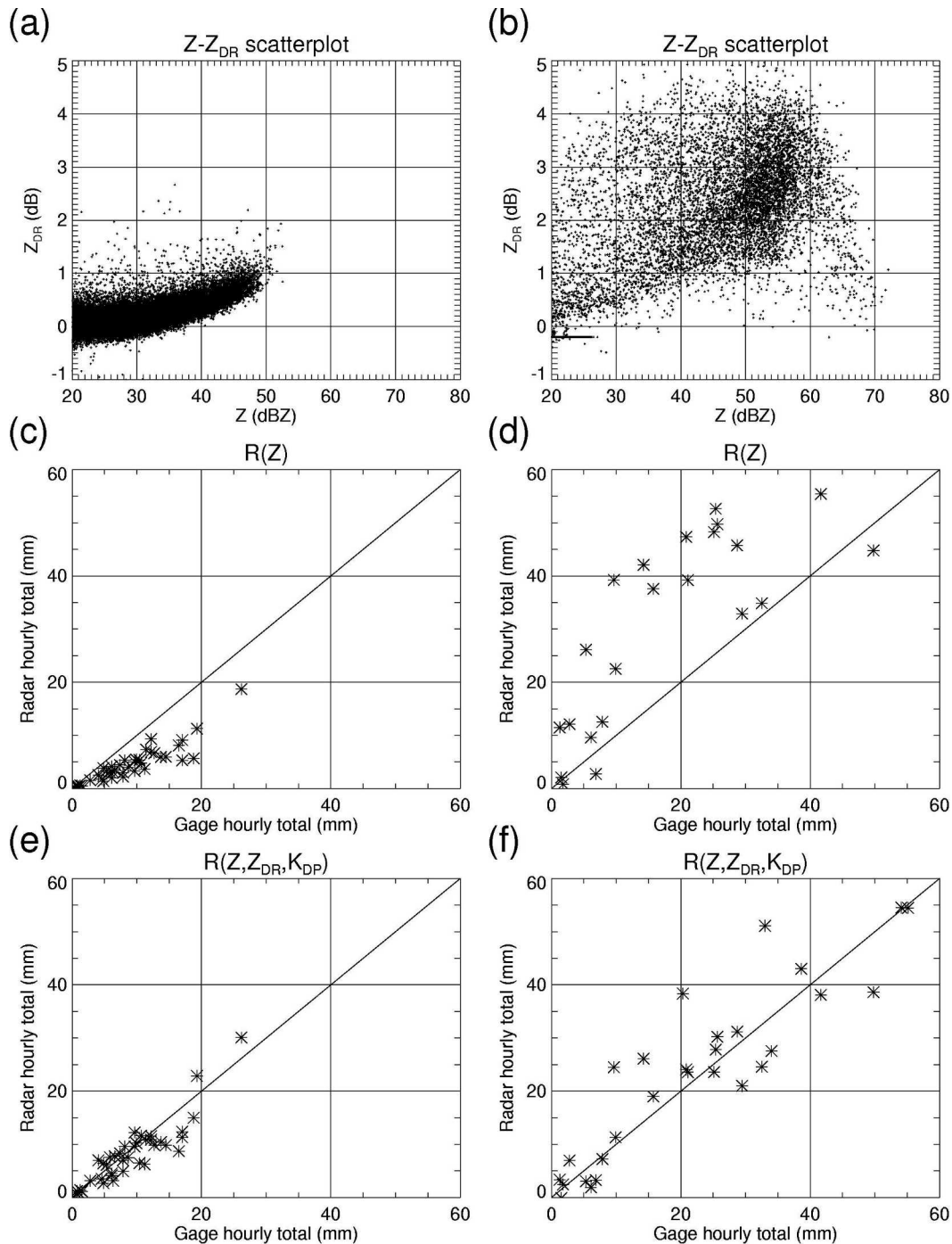


FIG. 11. Z - Z_{DR} scattergrams and hourly ARS gauge totals vs rainfall estimates from the $R(Z)$ and $R(Z, K_{DP}, Z_{DR})$ algorithms for tropical rain [(left) 1800–1900 UTC 8 Sep 2002] and rain mixed with hail [(right) 0700–0800 UTC 14 May 2003].

At distances less than 90 km from the radar where variability of raindrop spectra and possible presence of hail are dominant factors affecting the accuracy of rainfall estimation, most polarimetric algorithms clearly outperform the conventional one, although the degree

of improvement might be noticeably “weighted” by a few spring-heavy rain events.

The “synthetic” polarimetric algorithm $R(Z, K_{DP}, Z_{DR})$ shows the best performance. This algorithm is most robust with respect to radar calibration errors,

DSD variations, uncertainty of the raindrop shapes, and the possible presence of hail. The rms error of the 1-h total estimate is reduced by a factor of 1.7 for point measurements and a factor of 3.7 for areal rainfall estimates.

The most significant improvement is achieved in areal rainfall estimation and in measurements of heavy precipitation (often mixed with hail).

These advantages have important practical implications for (a) river flash-flooding forecasts and management that require reliable measurement of areal rain accumulations regardless of rain intensity, and (b) urban flash-flooding forecasts that requires accurate estimation of heavy rain with a high spatial resolution.

Acknowledgments. The authors acknowledge funding support for this work from the U.S. National Weather Service, the Federal Aviation Administration, and the Air Force Weather Agency through the NEXRAD Product Improvement Program. Additional funding came from the National Science Foundation Grant ATM-9907930.

Special thanks are conveyed to the personnel of the USDA Agricultural Research Service and Oklahoma Climatological Survey for providing high-quality rain gauge data.

REFERENCES

- Andsager, K., K. V. Beard, and N. F. Laird, 1999: Laboratory measurements of axis ratios for large drops. *J. Atmos. Sci.*, **56**, 2673–2683.
- Beard, K. V., and C. Chuang, 1987: A new model for the equilibrium shape of raindrops. *J. Atmos. Sci.*, **44**, 1509–1524.
- Brandes, E. A., A. V. Ryzhkov, and D. S. Zrnica, 2001: An evaluation of radar rainfall estimates from specific differential phase. *J. Atmos. Oceanic Technol.*, **18**, 363–375.
- , G. Zhang, and J. Vivekanandan, 2002: Experiments in rainfall estimation with a polarimetric radar in a subtropical environment. *J. Appl. Meteor.*, **41**, 674–685.
- Bringi, V. N., and V. Chandrasekar, 2001: *Polarimetric Doppler Weather Radar. Principles and Applications*. Cambridge University Press, 636 pp.
- , —, J. Hubbert, E. Gorgucci, W. Randeu, and M. Schoenhuber, 2003: Raindrop size distribution in different climate regimes from disdrometer and dual-polarized radar analysis. *J. Atmos. Sci.*, **60**, 354–365.
- Chandrasekar, V., E. Gorgucci, and G. Scarchilli, 1993: Optimization of multiparameter radar estimates of rainfall. *J. Appl. Meteor.*, **32**, 1288–1293.
- Crum, T. D., R. L. Albery, and D. W. Burgess, 1993: Recording, archiving, and using WSR-88D data. *Bull. Amer. Meteor. Soc.*, **74**, 645–653.
- Doviak, R. J., V. Bringi, A. V. Ryzhkov, A. Zahrai, and D. S. Zrnica, 2000: Considerations for polarimetric upgrades to operational WSR-88D radars. *J. Atmos. Oceanic Technol.*, **17**, 257–278.
- Fulton, R., A. Ryzhkov, and D. Zrnica, 1999: Areal rainfall estimation using conventional and polarimetric radar methods. Preprints, *29th Int. Conf. on Radar Meteorology*, Montreal, QC, Canada, Amer. Meteor. Soc., 293–296.
- Giangrande, S. E., and A. V. Ryzhkov, 2003: The quality of rainfall estimation with the polarimetric WSR-88D radar as a function of range. Preprints, *31st Int. Conf. on Radar Meteorology*, Seattle, WA, Amer. Meteor. Soc., 357–360.
- Goddard, J., K. Morgan, A. Illingworth, and H. Sauvageot, 1995: Dual-wavelength polarization measurements in precipitation using the CAMRA and Rabelias radars. Preprints, *27th Conf. on Radar Meteorology*, Vail, CO, Amer. Meteor. Soc., 196–198.
- Gorgucci, E., G. Scarchilli, and V. Chandrasekar, 1999: A procedure to calibrate multiparameter weather radar using properties of the rain medium. *IEEE Trans. Geosci. Remote Sens.*, **37**, 269–276.
- , —, —, and V. Bringi, 2000: Measurement of mean raindrop shape from polarimetric radar observations. *J. Atmos. Sci.*, **57**, 3406–3413.
- Heinselman, P. L., and A. V. Ryzhkov, 2004: Hail detection during the Joint Polarization Experiment. Preprints, *22d Conf. on Aviation, Range, and Aerospace Meteorology*, Hyannis, MA, Amer. Meteor. Soc., CD-ROM, J1.3.
- Illingworth, A., and T. Blackman, 2002: The need to represent raindrop size spectra as normalized gamma distributions for the interpretation of polarization radar observations. *J. Appl. Meteor.*, **41**, 286–297.
- Matrosov, S. Y., K. A. Clark, B. E. Martner, and A. Tokay, 2002: Measurements of rainfall with polarimetric X-band radar. *J. Appl. Meteor.*, **41**, 941–952.
- May, P., T. D. Keenan, D. Zrnica, L. Carey, and S. Rutledge, 1999: Polarimetric radar measurements of tropical rain at 5-cm wavelength. *J. Appl. Meteor.*, **38**, 750–765.
- Melnikov, V., D. Zrnica, R. Doviak, and J. Carter, 2003: Calibration and performance analysis of NSSL's polarimetric WSR-88D. NSSL Rep., 77 pp.
- Ryzhkov, A., and D. Zrnica, 1995: Precipitation and attenuation measurements at a 10 cm wavelength. *J. Appl. Meteor.*, **34**, 2121–2134.
- , and —, 1996: Assessment of rainfall measurement that uses specific differential phase. *J. Appl. Meteor.*, **35**, 2080–2090.
- , and T. J. Schuur, 2003: Effective shape of raindrops. Polarimetric radar perspective. *Proc. IGARSS-2003*, Toulouse, France, Geoscience and Remote Sensing Society, CD-ROM.
- , D. S. Zrnica, and R. Fulton, 2000: Areal rainfall estimates using differential phase. *J. Appl. Meteor.*, **39**, 263–268.
- , T. J. Schuur, and D. S. Zrnica, 2001: Testing a polarimetric rainfall algorithm and comparison with a dense network of rain gauges. *Proc. Fifth Int. Symp. on Hydrological Applications of Weather Radar*, Kyoto, Japan, 159–164.
- , S. E. Giangrande, and T. J. Schuur, 2003: Rainfall measurements with the polarimetric WSR-88D radar. National Severe Storms Laboratory Rep., 98 pp.
- , —, V. M. Melnikov, and T. J. Schuur, 2005: Calibration issues of dual-polarization radar measurements. *J. Atmos. Oceanic Technol.*, in press.
- Schuur, T. J., A. V. Ryzhkov, D. S. Zrnica, and M. Schoenhuber, 2001: Drop size distributions measured by a 2D video disdrometer: Comparison with dual-polarization data. *J. Appl. Meteor.*, **40**, 1019–1034.
- Zrnica, D., and A. Ryzhkov, 1996: Advantages of rain measurements using specific differential phase. *J. Atmos. Oceanic Technol.*, **13**, 454–464.